Journal of the Meteorological Society of Japan, Vol. 72, No. 6, pp. 873–884, 1994

A Numerical Study on the Formation of Organized Convective Storms: Part II. Dependence of "Broken-Line Formation" of Squall Line on its Line Direction

By Ryohei Misumi[1], Takao Takeda, Marjan Divjak[2] and Shuichi Tanahashi[3]

Institute for Hydrospheric-Atmospheric Sciences, Nagoya University, Chikusa-ku, Nagoya 464-01, Japan

(Manuscript received 1 February 1993, in revised form 27 September 1994)

Abstract

The effects of the direction of the convective-cell arrangement on the efficiency of "broken-line formation" of a squall line has been studied through numerical experiments. As fundamental experiments, small thermals were established along a line at a constant interval, and their evolutions were examined by changing the line direction relative to the vertical shear vector. The results showed that the broken-line formation occurred most efficiently when the line had a certain angle with the shear vector. The analysis suggested that the key factor controlling this efficiency is the vertical shear component normal to the line. When the component is too large, the downdrafts from pre-existing cells disturb the formation of the band-shaped updraft of a squall line. When the component is too small, a squall line cannot form easily because the low-level convergence is too weak. Broken-line formation most efficiently occurs when the component is in the middle range. Similar results were found when the shear contained veering or when the cell interval was small.

As a more realistic case, we put initial thermals at random locations. In this case, squall lines formed frequently in the direction along which broken-line formation occurred efficiently in the fundamental experiment. These results suggest that there is some favorable orientation for an efficient broken-line formation, and that squall lines have a tendency to appear along that direction.

1. Introduction

Precipitating convective clouds sometimes organize a mesoscale band which is called a squall line. The structure and behavior of squall lines have been studied by many researchers (*e.g.*, Newton, 1950; Houze, 1977; Zipser, 1977; Ogura and Liou, 1980; Weisman *et al.*, 1988; Fovell and Ogura, 1988).

Bluestein and Jain (1985) classified the formation process of severe squall line observed in Oklahoma with the use of radar-echo patterns. They found four modes in the formation process. One of these modes is called the "broken-line formation", in which a line of discrete cells transforms into a solid squall line as new cells develop between the older cells. In their analysis, 27 % of the severe squall lines formed through this process. This has frequently occurred when the atmosphere had a relatively large bulk Richardson number, namely large instability and a weak vertical shear. Bluestein *et al.* (1987) analyzed the formation process of non-severe squall lines by the same method. They found the same four formation modes. In their analysis, 36 % of the non-severe squall lines formed through broken-line formation. It can be said that broken-line formation is one of the major modes of squall-line formation regardless of its severity. In Japan, this mode was found in the formation process of the convective band observed by Takeda and Seko (1986) and the snow-band observed by Sakakibara *et al.* (1988).

The important dynamics of broken-line formation is the merging of discrete convective cells. Convective clouds have a property of merging together when they are close to each other. There are many studies on the merging process of convective clouds (*e.g.*, Simpson, 1980; Turpeinen, 1982; Tao and Simpson, 1984; Tao and Simpson, 1989; Westcott, 1994). According to them, convective clouds produce a "cloud bridge" just before they merge. Turpeinen (1982) simulated the merging process with the use of a three-dimensional nu-

1 National Research Institute for Earth Science and Disaster Prevention, Tennohdai 3-1, Tsukuba 305, Japan
2 Hydrometeorological Institute of Slovenia, Ujubljana
3 Fujitsu Corporation, Shinkamata 1-17-25, Ohta-ku, Tokyo 144, Japan

merical model. He showed that cloud bridges are produced by the interaction of downdraft outflows. A more realistic simulation by Tao and Simpson (1989) supported the results of Turpeinen (1982). Although their simulation did not refer to squall-line formation, the formation of a cloud bridge can explain how discrete cells develop into a solid squall line.

Bluestein and Jain (1985) pointed out another interesting fact about squall-line formation. They suggested systematic relations between the squall-line direction and the direction of the vertical shear vector. As for the average of the broken-line formation, the squall lines were perpendicular to the shear vector below the level of 1 km and at an angle of roughly 30°–40° with the shear vector between the level of 3 km and 7 km. This relationship was almost unchanged when they averaged the hodographs with a coordinate system whose axis was along the squall lines. This indicates that there exists a strong relationship between the direction of the shear vector and broken-line formation. However, it remains unknown why the broken-line formation has a relation with vertical shear direction.

A hypothetical explanation which can be considered is that the efficiency of a broken-line formation is strongly dependent on the direction relative to the shear vector. If a broken-line formation efficiently occurs when the cells are aligned in a certain direction, the squall lines directed to that orientation must appear most frequently. However, the influence of the direction of convective-cell arrangement on the broken-line formation has not been studied.

In this study we investigate the effects of the direction of convective-cell arrangement on the efficiency of broken-line formation with the use of a three-dimensional numerical model. Several experiments are performed by giving the broken-line of cells various directions relative to the shear vector. How the efficiency of broken-line formation changes is discussed.

2. Design of experiments

The numerical model used in this study is the same as in Part I (Misumi *et al.*, 1994), and is assumed to be non-hydrostatic and anelastic. The size of the numerical domain and boundary conditions are illustrated in Fig. 1. Horizontal sizes of the domain are 28 km and 150 km in the x- and y-direction, respectively. Cyclic boundary conditions are used in the x-direction, while open boundary conditions as in Part I are used in the y-direction. The vertical size of the domain is 15 km, and the upper and lower boundaries are rigid and air slips freely. Grid sizes are 2 km in the horizontal direction and 0.5 km in the vertical direction.

As an initial disturbance, two small thermals are established along the x-axis at the 0.25 km level at

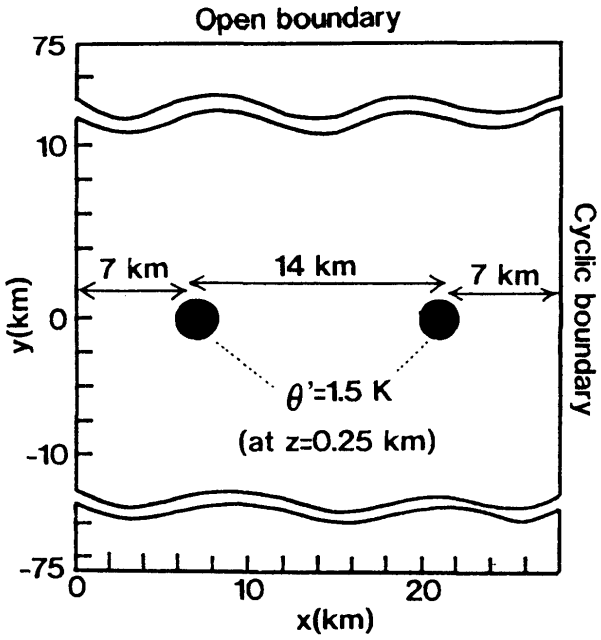

Fig. 1. Schematic illustration of the model domain, lateral boundary conditions and initial disturbance for Cases A–C.

$y = 0$. Because the lateral boundary conditions for the x-direction are cyclic, a broken-line of cells which has an infinite length along the x-axis appears. Each thermal is warmer by 1.5 K than the surrounding air and their horizontal sizes are 2 km. The situation assumed in our experiment, that only two discrete thermals exist in the domain, is similar to that of Droegemeier and Wilhelmson (1985a, b). They discussed the behavior of storms initiated by the outflow interaction, but they did not refer to squall-line formation. Our main interest is in the formation of squall lines from the two discrete cells and its dependence on the direction of the cells.

Some attention is needed to determine the interval of the thermals, since this is one of the important factors which will affect the efficiency of the squall-line formation. If it is too large, the cells do not interact and a squall line will not form. If it is too small, it is equivalent to giving a band-shaped storm initially. According to the numerical simulation by Tao and Simpson (1989), discrete convective cells interact when they are approximately 10 km to 20 km apart in distance. The radar-echo pattern shown by Bluestein and Jain (1985) indicated that the intervals of the cells were in a range from a few km to 30 km when broken-line formation occurred. In the present experiment, the thermals are placed at 14 km intervals in the control case, and the effects of the thermal intervals are examined by sensitivity tests.

The initial atmosphere is horizontally homoge-

neous. The vertical profiles of the temperature and relative humidity are the same as in Case A in Part I, except for the relative humidity in the lower layer. In this study, the relative humidity is 70 % at the surface and linearly increases up to 90 % to the LFC (level of free convection) at the 1.25 km level. CAPE (convective available potential energy) and CIN (convective inhibition) are 3500 m^2/s^2 and 15 m^2/s^2, respectively. CAPE is large relative to the observation by Bluestein and Jain (1985) (2820 m^2/s^2 in average) but the simulated clouds showed realistic behavior, since a part of the convective energy was diffused due to some incompleteness of the numerical model, such as the large diffusion coefficient or the coarse horizontal grid. The pressure at the surface is 1000 hPa and a hydrostatic balance is assumed initially.

Five sets of experiments are made: Cases A–E. Wind hodographs in Cases A, B and C are shown in Fig. 2. In Case A the atmosphere has a unidirectional vertical shear, its strength is 1 ms^{-1}/km from the surface to the 6 km level, and the wind velocity above the 6 km level is constant. In this case, five runs (A1–A5) are performed by changing the direction of the shear vector. The angle between the shear vectors and x-axis are 0°, 22.5°, 45°, 67.5° and 90°, respectively. Because no orography is assumed, the environmental conditions for the storms are identical for all runs; the only difference is the direction of the line of cells relative to the vertical shear vector. Effects of the line directions of the cells are examined in this case.

In Case B the vertical shear below the 6 km level is stronger than in Case A; 1.5 ms^{-1}/km. The vertical shear vector in B1 and B2 has the same y- and x-component as A2; only the x- and y-components of the shear vector are changed from A2. As will be shown in later, the broken-line formation of A2 occurred most efficiently in Case A. Case B is made in order to examine which vertical shear component was more important for the efficient squall-line formation in A2.

In the real atmosphere, vertical shear usually contains some veering. In Case C, the vertical shear vectors turn their direction at the 3 km level. The strength of the vertical shear averaged from the surface to the 6 km level is the same as in Case A. Five runs are performed by changing the vertical shear direction. In this case, effects of vertical shear veering are examined.

In Case D the wind fields are the same as in Case A; wind fields in D1, D2, ··· and D5 correspond to those in A1, A2, ··· and A5, respectively. In this case the intervals of the initial thermals are changed from Case A. The thermals are given at 8 km intervals instead of 14 km. The horizontal size of the domain is extended to 32 km in the x-direction in order to keep a constant interval. Effects of cell

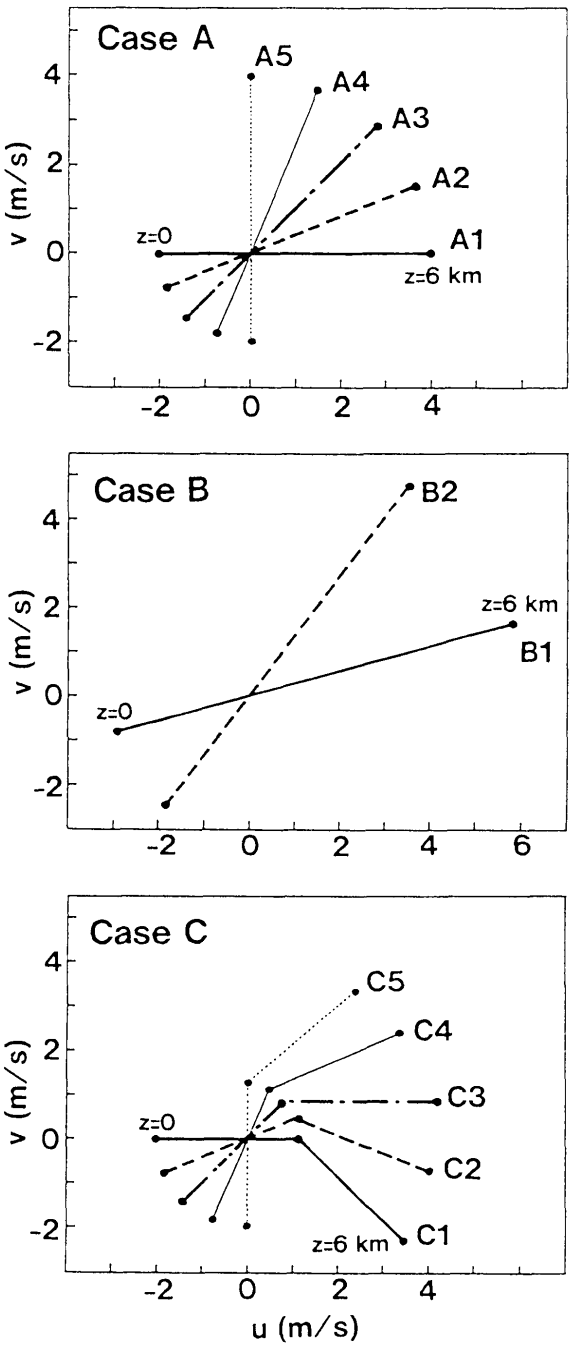

FIg. 2. Initial wind hodographs for Cases A–C.

intervals on broken-line formation are examined in this case.

In Cases A–D, the broken-line of thermals lying at constant intervals are given as initial disturbances. In the real atmosphere, however, convective cells are not always arranged at constant intervals. Moreover, the other cells usually exist near the broken-line of cells. The influences of these factors should be examined. As a more realistic case, initial thermals are arranged at random places in Case E in a similar way to Part I. The horizontal size of the domain in extended to 150 km × 150 km. Open boundary con-

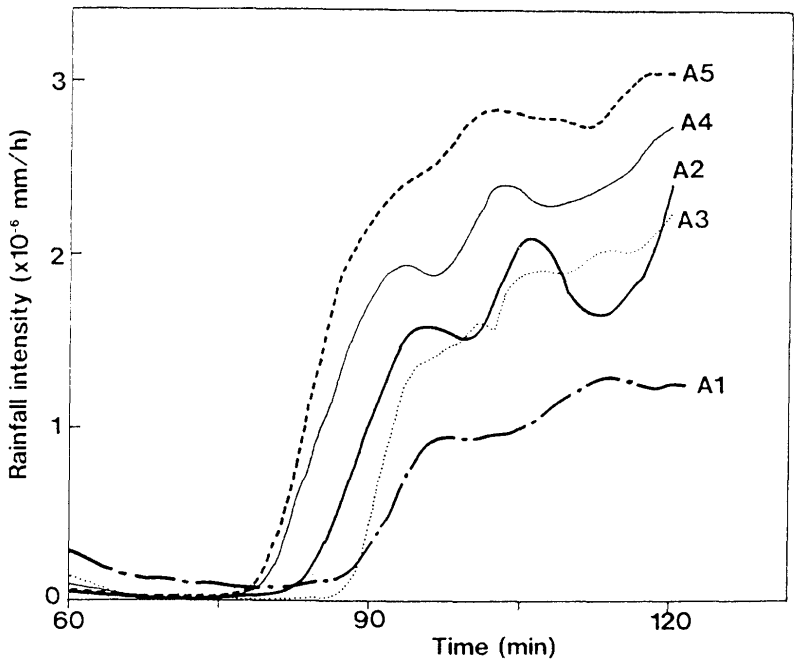

Fig. 3. Time variations of rainfall intensity for Case A, averaged for the domain where $y > 0$.

ditions are used for lateral boundaries. The thermals are given near the center of the domain to avoid the noise from the lateral boundaries. The initial wind in this case is the same as in A1; the shear vector is along the x-axis. In case E, a total of ten runs are performed by changing the initial thermal patterns. In this case we will see whether the results in Cases A–D hold true or not under more realistic condition.

The computation is made for 120 minutes in every run.

3. Results in Case A

a. Precipitation patterns

In every run in Case A, the initial thermals developed into precipitating convective cells. These cells produced precipitation after about 30 min. They decayed near 60 min and secondary cells formed around 75 min. Figure 3 shows time variations of rainfall intensity after 60 min. It shows the intensities averaged in positive y-regions, since the secondary cells developed vigorously on this side. In every run, the rainfall intensity became large around 75 min with the formation of secondary cells, and shows small variation after 105 min. The rainfall intensity after 90 min is largest in A5 and smallest in A1. This is because the vertical shear vector in A5 has so large a y-component that a large amount of warm and moist air enters into the storm.

Figure 4 shows horizontal distributions of a vertically integrated precipitating-water content in A1, A2 and A5. At 30 min considerable precipitation is found at the location where the initial thermals were given. At 102 min, the precipitating water is distributed in a band in A2, while it remains in broken-line-like distributions in A1 and A5. The band-shaped precipitation in A2 persists at 117 min. On the other hand, precipitating water in A1 and A5 still remains as broken lines at this time.

Secondary cells were also found in the negative y regions (not shown in Fig. 4), but they were much weaker than those on the positive side, except for A1 (this case is symmetric with respect to the x-axis). Precipitating water was distributed in cellular patterns in every run and no band-shaped storm formed.

In the present study a squall line is identified by the shape of the region enclosed by the 4 kg/m^2 contours of the vertically integrated precipitating water content (shaded region in Fig. 4). If the region shows a band longer than 25 km in length and smaller than 10 km in width, and if it keeps the shape longer than 15 minutes, it is called "a squall line". The threshold value of 15 minutes for the duration time of squall lines is also used by Bluestein and Jain (1985) and Bluestein *et al.* (1987). Transient line storms without the subsequent formation of new cells are excluded by the threshold.

Based on these criteria, a squall line formed in A2, while no squall line formed in A1 and A5. Also in A3 and A4, squall lines did not form until the end of the computation. These results do not always mean that squall lines never form under the conditions in A1, A3, A4 and A5, since the computations stopped before the storms reached their steady state. The results in this case should be regarded as showing that the squall line formed most efficiently under

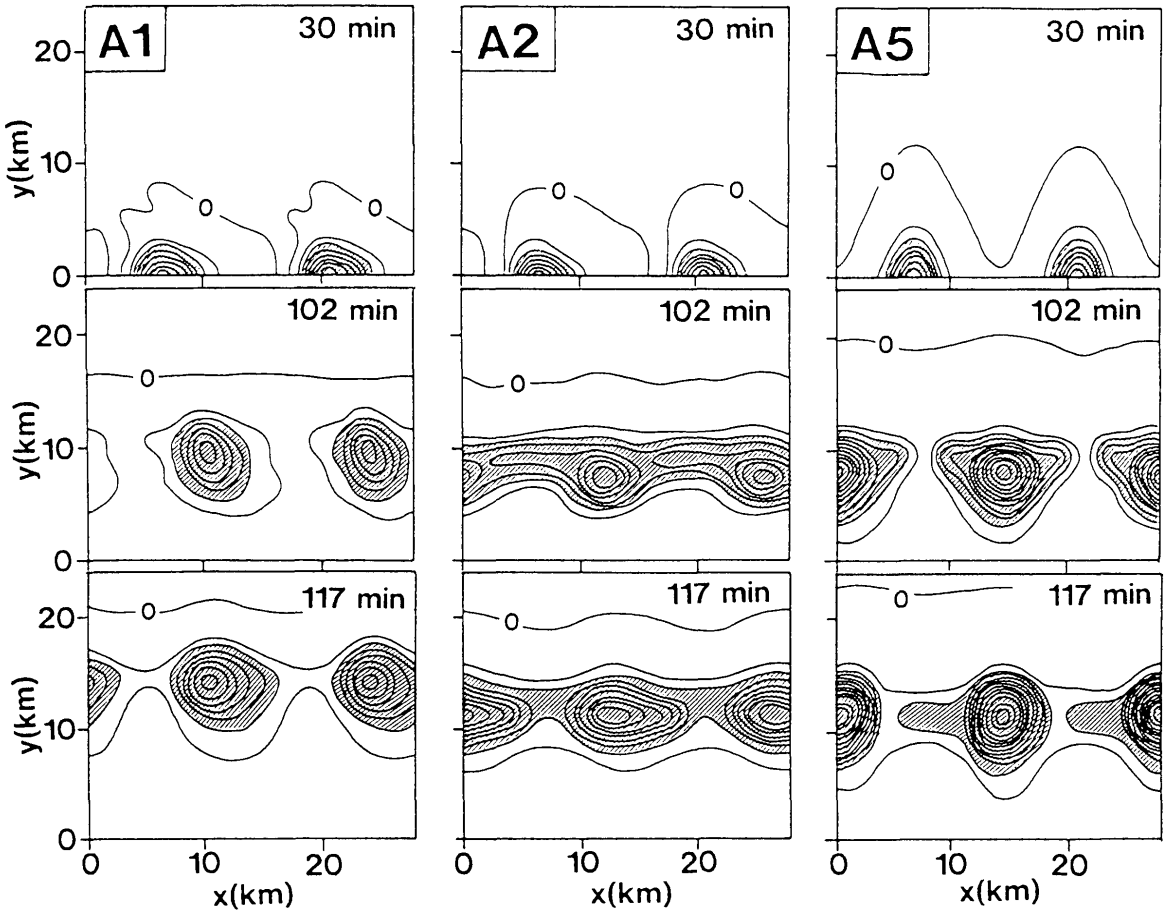

Fig. 4. Horizontal distributions of vertically integrated precipitating-water content at 30 min, 102 min, and 117 min for A1, A2 and A5. Only positive y regions are shown, because the main storms propagated in this direction. Contours are drawn every 2 kg/m^2. Shaded regions represent a larger value than 4 kg/m^2.

the condition of A2.

b. Storm structure

Figure 5 shows horizontal sections of vertical velocity (w) and wind vectors at the 6.5 km level in A1, A2 and A5. The wind velocities are averaged for 15 minutes from 105 min to 120 min to see their averaged structure. In the averaging process each numerical domain was moved in the positive y-direction with the same speed of the storm propagation. Distributions of positive w show similar patterns to those of precipitation (Fig. 4); A2 shows a band-shaped updraft, while A1 and A5 show a broken-line of updrafts.

Vertical cross sections for the squall line in A2 are shown in Fig. 6. These sections are along the line PQ in Fig. 5. The downdraft is located on the rear side (left side in the figure) of the updraft. A storm-relative horizontal wind shows a strong jet in the layer around the 4 km level. This middle-level jet is simulated by Fovell and Ogura (1988). They showed that it is the response to the pressure gradient in the middle level. Near the ground a strong rightward wind component is found. This corresponds to the gust at the squall front. θ' shows the existence of a cold-air pool near the surface. Large θ' are at almost the same location as the updraft. Precipitating water mainly falls on the rear side of the updraft. This structure is favorable for the persistence of the system since the loading of precipitating water does not disturb the development of the updraft. These features were found at all cross sections parallel to the y-axis, and are common to the squall lines and long-lived cumulonimbus clouds observed in many places (*e.g.*, Newton, 1950; Houze, 1977; Zipser, 1977; Ogura and Liou, 1980; Cotton and Anthes, 1989; Houze, 1993).

c. Evolution of the storms

As shown in Fig. 4, the broken-line of cells efficiently developed into a squall line in A2, while they remained as broken-line until the end of the computation in the remaining four runs. The difference in the storm evolutions is discussed.

Figure 7 shows horizontal sections of w and wind vectors at the 0.5 km level at 66 min. In each section

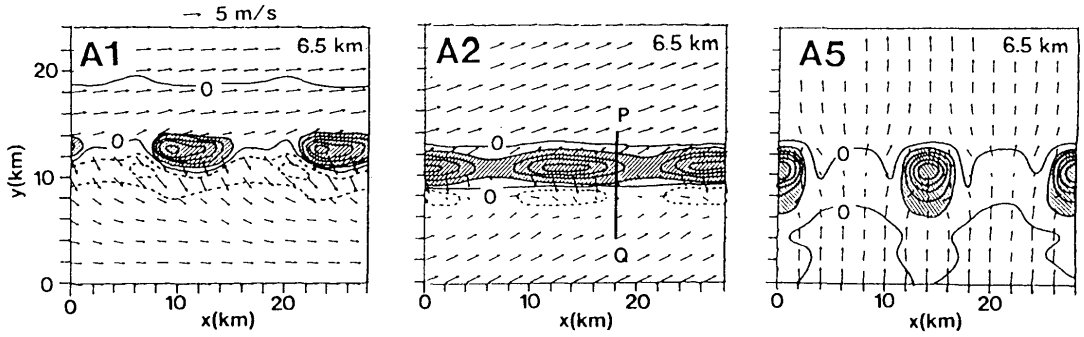

Fig. 5. Horizontal sections at the 6.5 km level of vertical velocity (w) and wind vectors averaged for 15 minutes from 105 min to 120 min. In the averaging process, the domain is moved in the positive y-direction at the same speed as the storm propagation. Contours of w are drawn every 2 m/s. Updrafts stronger than 2 m/s are represented by shaded regions.

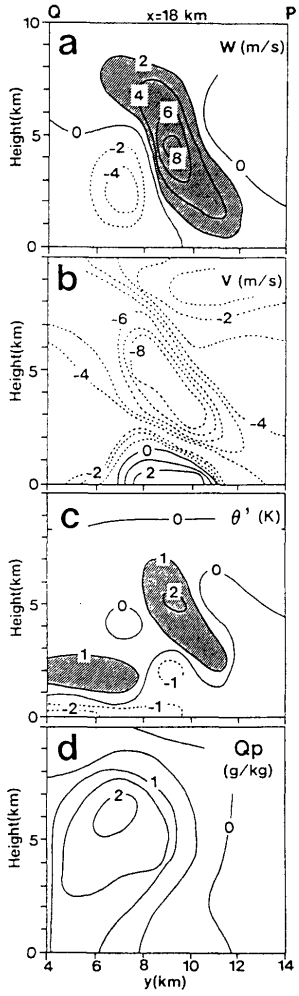

Fig. 6. Vertical cross sections along the line PQ in Fig. 5 of (a) vertical velocity (w; contoured every 2 m/s), (b) storm-relative horizontal wind component (v; contoured every 2 m/s), (c) potential temperature deviation from initial state (θ'; contoured every 1 K) and (d) mixing ratio of precipitating water (Qp; contoured every 0.5 g/kg).

the downdrafts around $x = 7$ km and 21 km originate from the initial cells. In every figure strong updrafts are found between the downdrafts. These updrafts are caused by the strong low-level convergence due to the interaction of the downdraft outflows. In A2 a strong band-shaped updraft is already organized at this time. On the other hand, the updrafts are distributed as broken-lines in A1 and A5. The difference in the patterns of w are similar to those at the 6.5 km level (Fig. 5) and to the precipitation patterns (Fig. 4).

Figure 8 shows distributions of horizontal divergence (div), divergence in the y-direction ($\partial v/\partial y$) and the x-direction ($\partial u/\partial x$) at the 0.5 km level at 66 min. Large negative divergences (shaded regions), namely, strong horizontal convergences, coincide with large w at the 0.5 km level (Fig. 7). In A1 the degree of convergence is small relative to A2, especially in the framed region (Area 1). Inside of Area 1 the absolute value of $\partial v/\partial y$ is much smaller than that in the corresponding region in A2, while $\partial u/\partial x$ shows a similar value to A2. This indicates that the weak convergence in Area 1 results from the small convergence in the y-direction. Because the vertical shear vector of A1 does not have a y-component, the storm-relative wind from a positive y-direction is very weak in this run. This causes the weak low-level convergence in the y-direction, and such a weak low-level convergence in the y-direction is also found in A2.

The degree of the horizontal convergence in A5 is particularly weak in the framed region, Area 2. The absolute value of $\partial v/\partial y$ in this area is not as small as in Area 1. However, $\partial u/\partial x$ shows a positive value in Area 2. This indicates the existence of a strong divergence in the x-direction. The divergence offsets the convergence in the y-direction and makes horizontal convergence significantly weak in Area 2. The positive $\partial u/\partial x$ in Area 2 is produced by the downdraft of the convective cell located at $x = 21$ km. Because the shear vector of A5 has a large positive

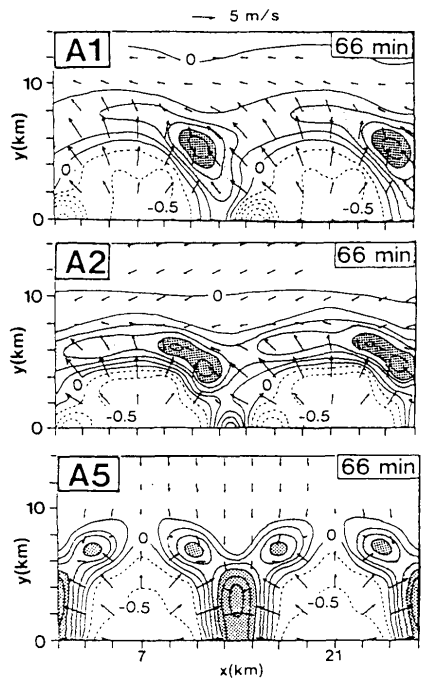

Fig. 7. Horizontal cross sections at 0.5 km of w and wind vectors for A1, A2 and A5 at 66 min. Contours of w are drawn every 0.25 m/s. Dark and light shaded regions represent updrafts stronger than 1 m/s and 0.5 m/s, respectively.

y-component, the downdraft of the convective cell is elongated to a positive y-direction and disturbs the convergence inside of Area 2. It locally prevented the updraft formation along the gust front. Also, in A3 and A4, the downdrafts from initial cells disturbed the formation of band-shaped updrafts.

The y-component of the shear vector in A2 is large enough to make a strong low-level convergence and small enough for the downdrafts not to disturb the band-shaped convergence. In this run a band-shaped updraft was produced along the gust front and a squall line formed.

4. Sensitivity tests

a. x- and y-components of the shear vector

In Case A broken-line formation occurred most efficiently when the initial line of the cells had a certain angle to the vertical shear vector (A2). The analysis of the divergence filed suggested that the y-component of the vertical shear vector, namely, the normal component of the shear vector to the line, was the key factor which controlled the efficiency of the broken-line formation. When the component was too small, a squall line did not form because low-level convergence along the gust front was too weak (A1). When the component was too large, the downdrafts from initial cells disturbed the band-shaped updraft formation (A3, A4 and A5). Case

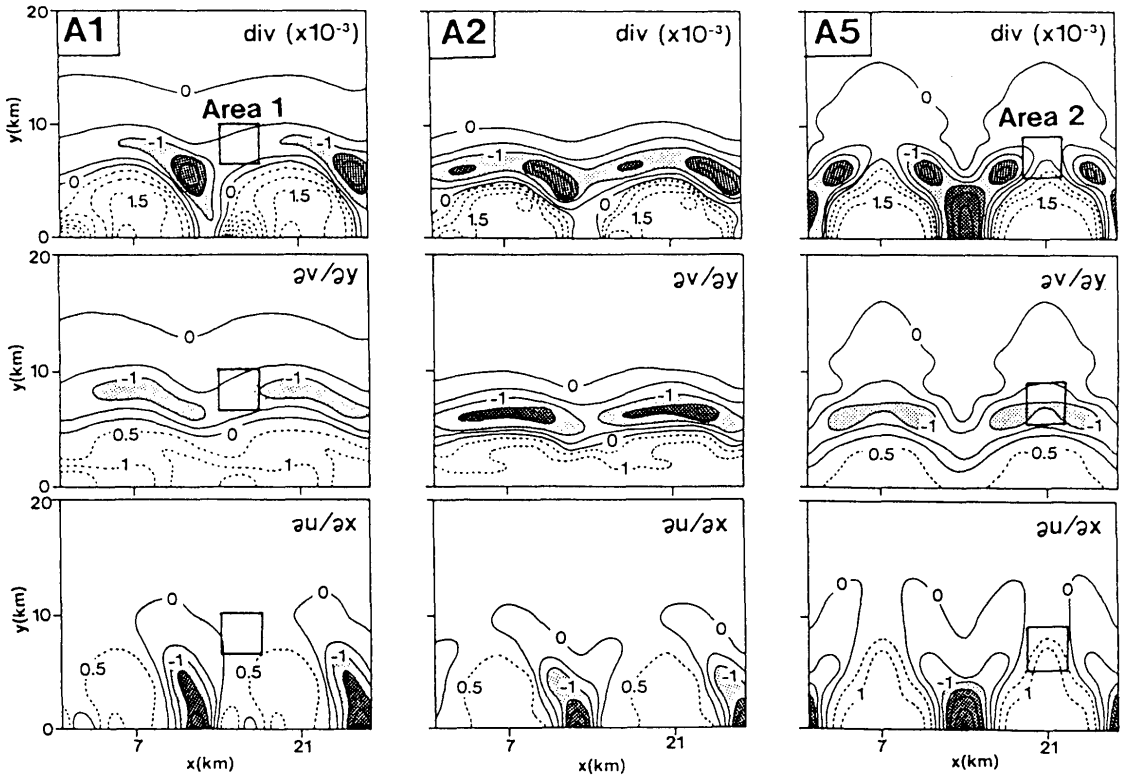

Fig. 8. Horizontal sections at the 0.5 km level of horizontal divergence (div), divergence in the y-direction ($\partial v/\partial y$) and in the x-direction ($\partial u/\partial x$) at 66 min. Contours are drawn every 0.5×10^{-3} s^{-1}. Light and dark shaded regions represent horizontal convergences larger than 1×10^{-3} s^{-1} and 1.5×10^{-3} s^{-1}, respectively.

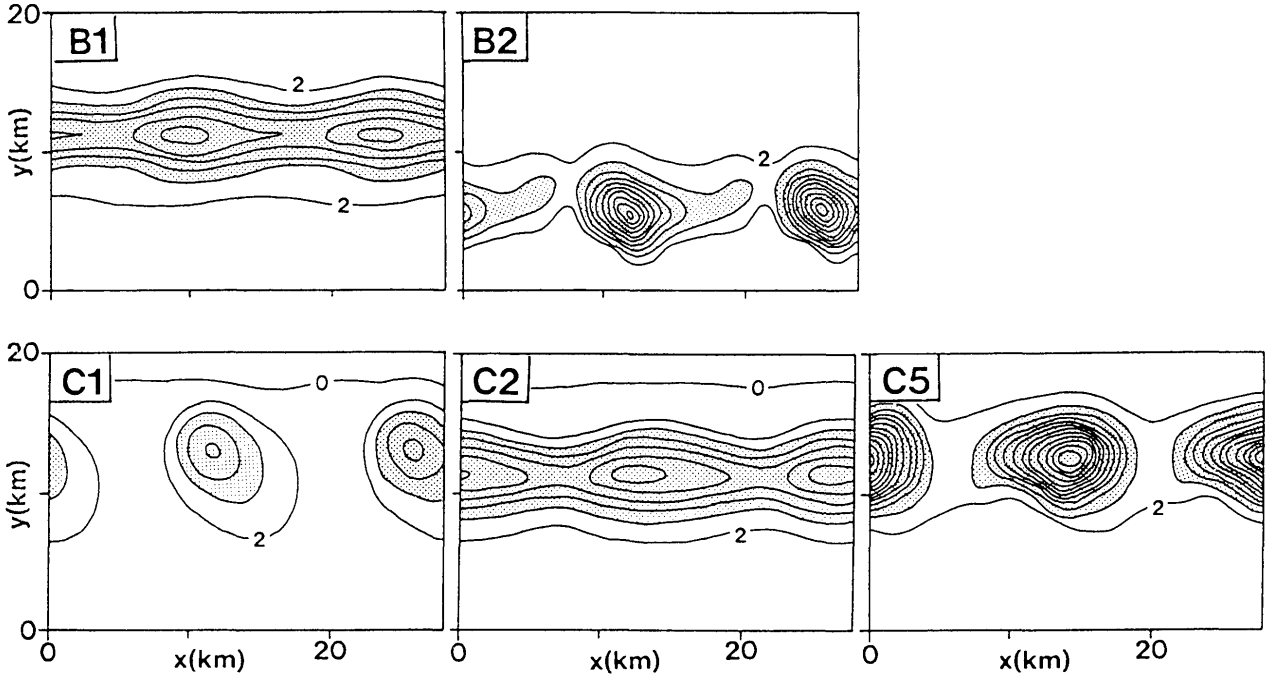

Fig. 9. Same as Fig. 4, except for B1, B2, C1, C2 and C5 at 120 min.

B was set up in order to ascertain that the normal shear component was the main factor which affected the difference in the squall-line formation in Case A. The vertical shear in B1 has the same y-component as in A2, while B2 has the same x-component as in A2. In these runs only the x- or y-component of the shear vector is different from A2.

Horizontal distributions of the vertically integrated precipitating-water content for B1 and B2 at 120 min are shown in the upper part of Fig. 9. In B1, which has the same y-component as A2, a squall line efficiently formed, as in A2. On the other hand, no squall line formed in B2. In B2, which has a larger y-component in the vertical shear, the downdrafts prevented the formation of a band-shaped updraft as in A3–A5. These results support the thesis that the main factor that contributed to the efficient broken-line formation in A2 was the y-component of the shear vector.

However, the results suggest that the x-component of the vertical shear also has some effect on the efficiency of broken-line formation. The squall line in B1 formed earlier (at 81 min) than that in A2 (at 96 min), although the y-components were the same. It is considered that a larger x-component promotes a more efficient broken-line formation.

b. Wind shear veering

In Cases A and B the wind fields had unidirectional vertical shears. In the real atmosphere, however, vertical shear usually contains some veering. It is necessary to perform the same experiment under the condition in which the vertical shear is veering. Vertical shear in Case C changes direction at the 3 km level (Fig. 2). Five runs were performed by changing the direction of the shear vectors.

Distributions of the vertically integrated precipitating-water content at 120 min for C1, C2 and C5 are shown in the lower part of Fig. 9. A squall line formed in C2, in which the vertical shear direction below the 3 km level was the same as in A2. On the other hand, squall lines did not form in the remaining runs. The failure of squall-line formation in these runs was for the same reason as in Case A, namely, the low-level convergence was too weak in C1, while downdrafts from initial cells disturbed the updraft formation in C3–C5.

In Case C, however, the vertical shear direction most favorable for the efficient broken-line formation was slightly different from Case A. Although the averaged vertical shear between the surface to the 6 km level in C3 was the same as in A2, a squall line did not form in this run. On the other hand, in C2, which has the same vertical shear as A2 only below the 3 km level, a squall line efficiently formed. This implies that the vertical shear in the lower layer has a larger influence on broken-line formation than in the upper layer.

c. Cell intervals

In Case D only the interval of initial thermals is different from Case A. Distributions of vertically integrated precipitating-water content at 81 min and 105 min for D1, D2 and D5 are shown in Fig. 10. A squall line formed earliest in D2. Precipitating water organized into a band at 81 min and persisted to the

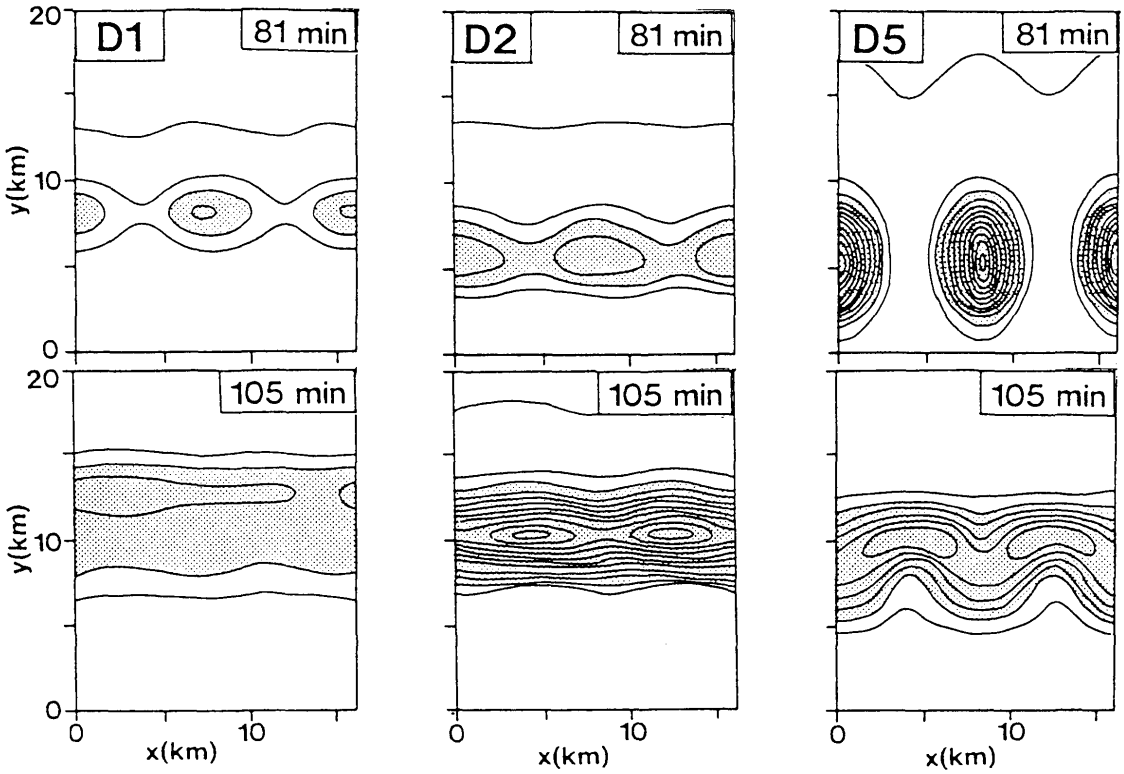

Fig. 10. Same as Fig. 4, except for D1, D2 and D5 at 81 min and 105 min.

end of the computation. In D1, though it had the same wind field as A1, a squall line formed at 105 min. In this run the outflow from the cold-air pool was stronger than A1 because the precipitating cells were closer to each other. It produced a strong horizontal convergence, enough to build a band-shaped updraft. A squall line also formed in D5 at 105 min. In the earlier stage of D5, precipitating water was distributed in a broken line as in A5 (81 min). However, because the cold-air pool developed strongly, the gust front propagated so quickly that a band-shaped updraft formed without being disturbed by the downdrafts from pre-existing cells. Squall lines also formed in D3 and D4.

Squall lines are found in all the runs of this case. This implies that broken-line formation occurs more easily when the cell interval is small. However, the squall line in D2, which was in the same wind field as in A2, was produced most quickly in Case D. This indicates that the most favorable shear direction for an efficient broken-line formation is unchanged between Cases A and D.

5. Random-thermal experiment

In Cases A–D, a broken-line of cells lying at a constant interval was initially set up. In the real atmosphere, however, the cells are not distributed at a fixed interval. Moreover, other cells usually exist near the broken-line of cells. Case E examines the effects of these factors.

A typical result in this case is shown in Fig. 11. Because the initial thermals are distributed at random locations, many broken lines which have various orientations and various cell intervals exist simultaneously. In Fig. 11, a squall line formed at 102 min. This squall line formed from a broken line of cells labelled f1, f2, f3 and f4. It should be noted that the direction of the broken line f1–f4 is approximately 20°–40° with the vertical shear vector (along the x-axis). The direction of the line relative to the shear vector is very similar to that in A2, in which broken-line formation occurred most efficiently. Although various directions of broken lines exist simultaneously, squall-line formation occurred only among these cells.

The frequency distribution of the squall-line directions in the ten runs of this case is shown in Fig. 12. Because the squall lines were not always a complete line shape, the direction was defined as the angle between the x-axis and the line connecting both edges of the band. Eight squall lines formed in this case. Most of the squall-line directions are in the range of 15°–30°, which is similar to the angle between the squall line in A2 and the shear vector (22.5°). This suggests that the line direction favorable for an efficient broken-line formation is hardly changed even when the cells are randomly distributed, and that squall lines tend to appear along that direction.

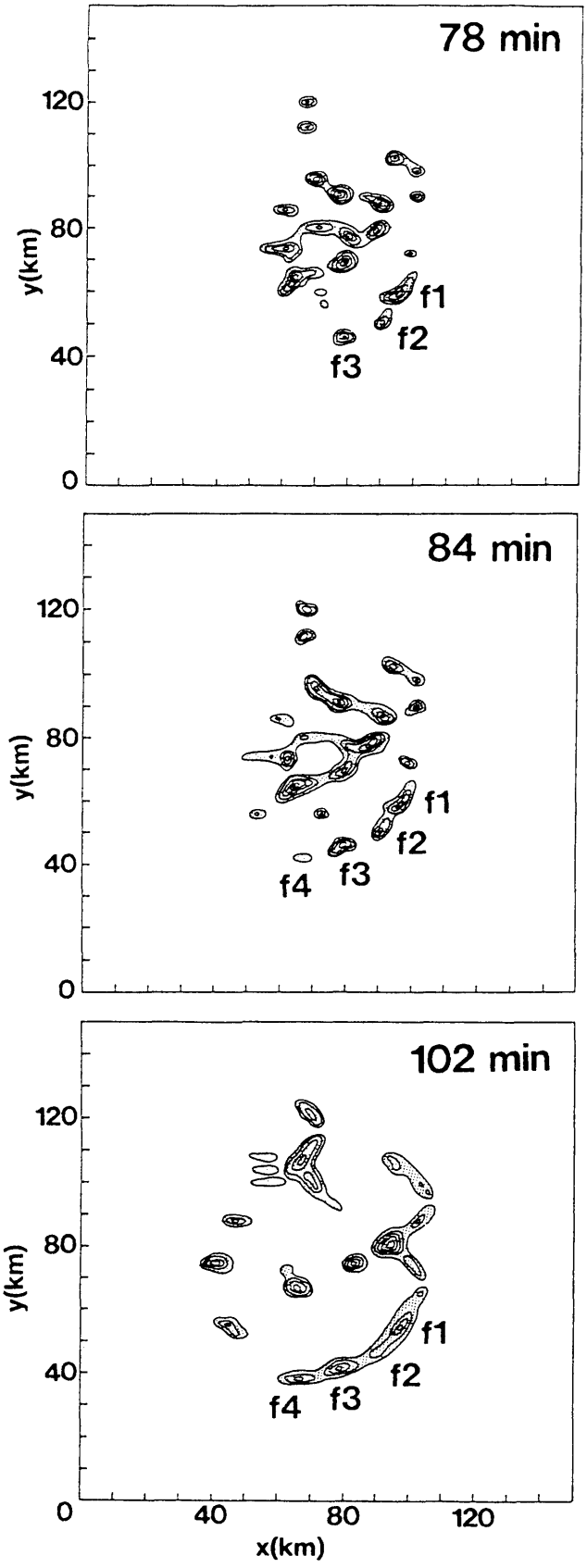

Fig. 11. Same as Fig. 4, except for Case E at 78 min, 84 min and 102 min. Contours are drawn every 4 kg/m^2 where the value is larger than 4 kg/m^2.

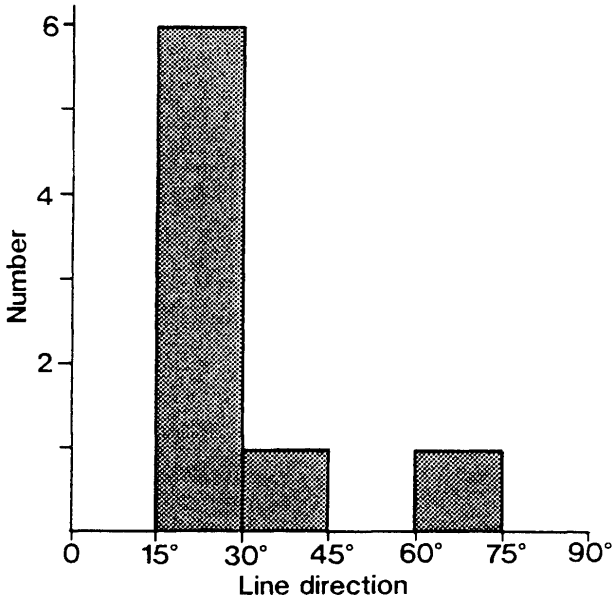

Fig. 12. Frequency distribution of squall-line directions relative to the x-axis for the then runs in Case E.

6. Summary and discussion

The effects of the direction of convective-cell arrangement on the efficiency of broken-line formation of a squall line was studied by numerical experiments. The results in Case A showed that broken-line formation occurred most efficiently when the cells were aligned in a certain direction relative to the vertical shear vector. The results of the analysis suggest that the key factor which controls the efficiency is the vertical shear component normal to the line; when the component was too large, formation of a band-shaped updraft was disturbed by the downdrafts from pre-existing cells. When the component was too small, low-level convergence was too small to produce a band-shaped updraft. Broken-line formation efficiently occurred when the component was in the middle range. Results of Case B supported this conclusion.

Similar results were found when the vertical shear turned its direction in the middle level (Case C). The results of Case C also suggested that the low-level vertical shear has larger effects on the efficiency of broken-line formation.

In Case D, the initial thermals were spaced at a smaller interval than in Case A. In this case squall lines formed in all the runs. This suggests that broken-line formation more easily occurs when the cell interval is small. However, the line direction most favorable for an efficient broken-line formation was unchanged from Case A.

In Case E, the thermals were located at random places in the same wind field as in Case A. Squall

lines frequently formed in the direction which was also the most favorable for the efficient broken-line formation in Case A. This result suggests that the favorable direction for an efficient broken-line formation is unchanged when the cells are distributed randomly, and that squall lines tend to appear along that direction.

In the present study, we showed that there is a favorable direction for efficient broken-line formation and squall lines frequently develop along this direction. However, this is not a direct explanation for the systematic relation between the squall-line direction and shear vectors pointed out by Bluestein and Jain (1985), because the effects of mesoscale disturbances are ignored in this study. Mesoscale disturbances, which are usually observed near squall lines, have a close relationship with both squall-line formation and ambient wind profiles. However, even if a mesoscale disturbance exists, cloud-scale dynamics are still considered to have large effects on the broken-line formation. We consider that the characteristic convective-cell interaction shown in the present study is an important factor which affects the formation of squall lines.

Acknowledgments

The authors wish to express their hearty thanks to the editor and the three reviewers for improving the original manuscript. Numerical calculations were carried out by using FACOM M-780 of Nagoya University and CRAY YMP-2 of the the National Research Institute for Earth Science and Disaster Prevention.

References

Bluestein H.B. and M.H. Jain, 1985: Formation of mesoscale lines of precipitation: Severe squall lines in Oklahoma during the spring. *J. Atmos. Sci.*, **42**, 1711–1732.

Bluestein H.B., G.T. Marx and M.H. Jain, 1987: Formation of mesoscale lines of precipitation: Nonsevere squall lines in Oklahoma during the spring. *Mon. Wea. Rev.*, **115**, 2719–2727.

Cotton, W.R. and R.A. Anthes, 1989: *Storm and cloud dynamics.* Intern. Geophys. Ser., 44, Academic Press, 843 pp.

Droegemeier, K.K. and R.B. Wilhelmson, 1985a: Three dimensional numerical simulations of deep convection produced by interacting thunderstorm outflows. Part I. Control simulation and low-level moisture variations. *J. Atmos. Sic.*, **42**, 2381–2403.

Droegemeier, K.K. and R.B. Wilhelmson, 1985b: Three dimensional numerical simulations of deep convection produced by interacting thunderstorm outflows. Part II. Variations in vertical wind shear. *J. Atmos. Sci.*, **42**, 2404–2414.

Fovell, R.B. and Y. Ogura, 1988: Numerical simulation of a midlatitude squall line in two dimensions. *J. Atmos. Sci.*, **45**, 3846–3879.

Houze, R.A., Jr., 1977: Structure and dynamics of a tropical squall-line system. *Mon. Wea. Rev.*, **105**, 1540–1567.

Houze, R.A., Jr., 1993: *Cloud dynamics.* Intern. Geophys. Ser., 53, Academic Press, 573 pp.

Misumi, R., M. Divjak, S. Tanahashi and T. Takeda, 1994: A numerical study on the formation of organized convective storms. Part I: Formation patterns of long-lasting cells. *J. Meteor. Soc. Japan*, **72**, 235–253.

Newton, C.W., 1950: Structure and mechanism of the prefrontal squall line. *J. Meteor.*, **7**, 210–222.

Ogura, Y. and M.T. Liou, 1980: The structure of a midlatitude squall line. *J. Atmos. Sci.*, **20**, 3144–3176.

Sakakibara, H., M. Ishihara and Z. Yanagisawa, 1988: Squall line like convective snowbands over the Sea of Japan. *J. Meteor. Soc. Japan*, **66**, 937–953.

Takeda, T. and K. Seko, 1986: Formation and maintenance of band-shaped convective radar echoes. *J. Meteor. Soc. Japan*, **64**, 941–951.

Tao, W.K. and J. Simpson, 1984: Cloud interactions and merging: numerical simulations. *J. Atmos. Sci.*, **41**, 2901–2917.

Tao, W.K. and J. Simpson, 1989: A further study of cumulus interactions and mergers: Three-dimensional simulations with trajectory analyses. *J. Atmos. Sci.*, **46**, 2974–3004.

Turpeinen, O., 1982: Cloud interactions and merging on day 261 of GATE. *Mon. Wea. Rev.*, **110**, 1238–1254.

Weisman, M.L., J.B. Klemp and R. Rottuno, 1988: Structure and evolution of numerically simulated squall lines. *J. Atmos. Sci.*, **45**, 1990–2013.

Westcott, N.E., 1994: Merging of convective clouds: Cloud initiation, bridging, and subsequent growth. *Mon. Wea. Rev.*, **122**, 780–790.

Zipser, E.J., 1977: Mesoscale and convective-scale downdrafts as distinct components of squall-line structure. *Mon. Wea. Rev.*, **105**, 1568–1589.

組織化した対流性ストームの形成過程に関する数値的研究
第2部. セルの並ぶ方向が、スコールラインの「破線型形成」の及ぼす影響について

三隅良平[1]・武田喬男・Marjan Divjak[2]・棚橋修一[3]
(名古屋大学大気水圏科学研究所)

セルの並ぶ方向が、スコールラインの「破線型形成」に及ぼす影響を、数値実験により調べた。まず基礎的実験として、初期に小さいサーマルを等間隔の破線状に与え、その向きをシアーベクトルに相対的にいろいろに変えて発達のしかたを比較した。その結果は「破線」の向きがシアーベクトルとある角度をなしたときに、スコールラインが最も効率よく形成することを示した。解析によると、このような効率の違いを支配する主要な因子は、鉛直シアーの破線に直交する成分である。この成分が大きすぎると、初期のセルからの下降流がスコールラインのバンド状上昇流の形成を妨げる。この成分が小さすぎると、下層の収束が弱いために、スコールラインが形成しにくい。シアー成分がその中間的な強さのときに、最も効率よく破線型形成がおこる。鉛直シアーが中層で向きを変えるケース、セルの間隔を変えたケースにおいても、同様の結果が得られた。

次により現実に近いケースとして、初期にサーマルをランダムな位置に与えた。このケースではある特定の向きをもったスコールラインが頻繁に形成し、その向きは基礎実験において効率よく破線型形成がおこった向きに一致していた。これらの結果は、効率よく破線型形成が起こる方向が存在し、スコールラインがその方向に沿って現れやすいことを示唆している。

[1]現在所属：防災科学技術研究所
[2]スロバニア水文気象研究所
[3]富士通株式会社